Paleoclimate model-derived thermal lapse rates: Towards increasing precision in paleoaltimetry studies

Journal Item

Earth and Planetary Science Letters 564 (2021) 116903

Contents lists available at ScienceDirect

Earth and Planetary Science Letters

www.elsevier.com/locate/epsl

Paleoclimate model-derived thermal lapse rates: Towards increasing precision in paleoaltimetry studies

Alex Farnsworth [a,*], Paul J. Valdes [a], Robert A. Spicer [b,c], Lin Ding [d,e], Caitlyn Witkowski [f], Vittoria Lauretano [f], Tao Su [c,e], Shufeng Li [c,e], Shihu Li [g], Zhekun Zhou [c,e]

[a] School of Geographical Sciences and Cabot Institute, University of Bristol, Bristol, BS8 1SS, UK
[b] School of Environment, Earth and Ecosystem Sciences, The Open University, Walton Hall, Milton Keynes, MK7 6AA, UK
[c] CAS Key Laboratory of Tropical Forest Ecology, Xishuangbanna Tropical Botanical Garden, Chinese Academy of Sciences, Mengla 666303, China
[d] Key Laboratory of Continental Collision and Plateau Uplift, Institute of Tibetan Plateau Research, and Center for Excellence in Tibetan Plateau Earth Sciences, Chinese Academy of Sciences, Beijing 100101, China
[e] University of Chinese Academy of Sciences, Beijing 100049, China
[f] School of Chemistry and Cabot Institute, University of Bristol, BS8 1TS, UK
[g] Lancaster Environment Centre, University of Lancaster, LA1 4YQ, UK

ARTICLE INFO

Article history:
Received 2 May 2020
Received in revised form 5 March 2021
Accepted 16 March 2021
Available online 31 March 2021
Editor: A. Yin

Dataset link:
http://www.bridge.bris.ac.uk/resources/simulations

Keywords:
palaeoclimate
palaeoaltimetry
palaeoclimate modelling
Tibetan geology

ABSTRACT

Quantifying how land surface height, such as that of the Tibetan region, has changed with time is crucial for understanding a range of Earth processes, including atmospheric dynamics, biotic evolution and tectonics. Elevation reconstructions are highly uncertain and controversial, in part because of assumptions used in their calculation. The largest uncertainties are in the choice of unconstrained thermal lapse rates. Thermal lapse rates are defined as a change in surface temperature with altitude and have long been used to estimate paleoelevation. If we know both the lapse rate and the temperature at two sites at different elevations, then in theory we can calculate their height difference. There are different types of lapse rates (Dry, Saturated, Environmental and Terrestrial), yet which is the most useful for paleoaltimetry is unknown. Previous paleoelevation studies have often used observed modern-day global annual mean free air or terrestrial thermal lapse rates to measure elevation change, with the assumption that observed modern-day lapse rates are similar to those of the past. Here, using the HadCM3L paleoclimate model we demonstrate that Eocene global mean free air and terrestrial thermal lapse rates are not only different from the modern, but also show little predictive skill in reproducing prescribed model topography. Free-air lapse rates are largely insensitive to increased pCO_2 (showing only a decrease of ~0.1-0.5 °C/km), whereas lapse rates at Earth's surface, the most applicable for fossil-based paleoaltimetry, differed significantly locally and globally in the past compared to the Pre-industrial. This suggests that modern terrestrial lapse rate expressions are inappropriate for tracking altitude changes through geologic time. Moist processes and resultant moisture content of airmasses play a critical role in much of this uncertainty. The use of a wet-bulb temperature-derived lapse rate reduces this uncertainty significantly improving the predictive skill. Local terrestrial thermal lapse rates can be useful in paleoaltimetry, but only through climate model mediation where uncertainties can be reduced and quantified. Critically, paleoclimate models offer the opportunity to provide mean sea-level surface temperature to derive an elevation estimate where proxy-based values may not be available.

1. Introduction

Mountain building has had a profound impact on climate through time. Understanding the spatiotemporal height and extent of mountain ranges in the geologic past is crucial because surface height will perturb the transfer of energy, mass and momentum, affecting local processes, such as monsoons (Acosta and Huber, 2020; Boos and Kuang, 2010; Sewall et al., 2000), silica weathering rates and biodiversity (Spicer et al., 2020a). Reconstruction of past mountains heights is not a straightforward undertaking. As the land surface rises it will cool, maintaining a fundamental thermodynamic relationship between temperature and altitude that is often preserved in fossil flora and fauna, as well as by geochemical

* Corresponding author.
E-mail address: alex.farnsworth@bristol.ac.uk (A. Farnsworth).

https://doi.org/10.1016/j.epsl.2021.116903

proxies. Potentially, this fossil-derived elevational change in temperature serves as a way of measuring surface height differences.

With two proxy-derived surface temperatures, one at sea level and one at height, a lapse rate can be employed to determine the height difference. A thermal lapse rate describes the change in temperature of a parcel of air with increasing altitude (°C/km) and can be defined as Γ = -dT/dz. Paleoaltimetry studies have often applied modern-day observed thermal lapse rates to estimate the difference in elevation between two locations, and often using differences in mean annual temperature (Axelrod, 1965; Axelrod and Bailey, 1976; Axelrod, 1997; Bai et al., 2018; Coffinet et al., 2017; Ehlers and Poulsen, 2009; Fluteau, 2003; Ghosh et al., 2006; Huntington et al., 2015; Jin et al., 2007; Meyer, 1992, 2007; Rowley, 2007; Schildgen et al., 2009; Wang et al., 2006). Feng and Poulsen (2016) showed the potential impact of utilising unconstrained modern lapse rates to estimate the Eocene height of the western North American Cordillera. Their results suggest that higher elevation surface heights were potentially underestimated by as much as 3 km.

Four types of lapse rates are commonly used:

i) A Dry adiabatic (Γd) lapse rate (9.8 °C/km). This is, the lapse that would result from a dry airmass rising through the atmosphere in hydrostatic equilibrium.

ii) A Saturated adiabatic (Γm) lapse rate. Γm varies between ∼4–9 °C/km depending on the temperature and pressure at air parcel saturation. The greater the moisture content of the air parcel, the greater the latent heat that can be released when condensation takes place, warming the air parcel. A lower moisture content, such as might be seen in a cooler climate, will lead to a larger Γm (nearer to a Γd), while a higher moisture content, (e.g. in a warmer climate in the Eocene), will decrease Γm. On average the modern global Γm is taken as ∼6.0 °C/km.

iii) Environmental lapse rate (Γe) is the lapse rate of non-rising air. As a global average, Γe is taken as 6.5 °C/km lapse rate (Barry and Chorley, 1987). This lapse rate occurs as part of the surrounding free-air atmosphere (environment), i.e. not in a rising air parcel, and is commonly used in paleoaltimetry studies. Γe calculated over just the land surface, Γe_t (ocean Γe removed from the calculation) may also differ from that of the global mean.

iv) Terrestrial (Γt) lapse rates. These are considered the most applicable lapse rate expression for paleoaltimetry studies (Meyer, 1992), and are measures of the temperature change along a surface transect near the land-surface-atmosphere interface, and are different from those of the free atmosphere as with Γe. Differences in surface albedo, soil heat capacity, vegetation cover, lower wind speeds (due to surface friction), and water vapour content (evapotranspiration) may all influence surface temperature. It is this temperature, derived from a paleontological or geochemical proxy, that has to be used to document past surface height changes. Γt is usually less than the Γe as a result of daytime heating of near-surface air on slopes (Meyer, 1992). A modern global average of 5.5 °C/km Γt (Axelrod and Bailey, 1976) has been generally assumed. However, Wolfe (1992) showed that Γt can vary significantly as both a function of altitude (0.3–3.6 °C/km) within the same climate zone, as well as latitude (−4.9 to 4.5 °C/km), casting doubt on the validity of using a standard global terrestrial lapse rate.

Use of any of these lapse rates will lead to potentially significantly divergent paleoelevation reconstructions, and it is yet to be conclusively shown which is the most appropriate and accurate.

Lapse rates (Γm, Γe, Γt) are not spatially uniform, as established from modern-day in-situ observations (Rolland, 2003; Minder et al., 2010), and vary due to factors such as incident solar radiation as a function of latitude, slope and aspect (Wolfe, 1992), atmospheric stability, moisture content (Zamora et al., 2016), and ground surface albedo (Sewall et al., 2000). All these factors exert dissimilar thermodynamic profiles on the local atmosphere and can modify the thermal profile on a airmass from its source to deposition. Unfortunately, many of these influences are unquantifiable from paleo-proxy records, meaning paleoaltimetry studies often contain a high degree of uncertainty simply in relation to the chosen lapse rate (usually a modern analogue). Thus, surface-height estimates based on lapse rate arguments remain highly uncertain and controversial.

In addition to spatial uncertainty in lapse rates there is also a temporal component that is neglected. Lapse rates are determined by the surrounding environment (climate, land surface processes, teleconnections) all of which can vary on different time scales from e.g. (diurnal (Kattel et al., 2015), seasonal (Minder et al., 2010), inter-annual (Thayyen and Dimri, 2018), and geologic (Su et al., 2019)).

It is unknown how lapse rates respond to changes in atmospheric composition (CO_2 and aerosols), solar insolation and paleogeography. Moreover, the potential importance and quantification of seasonal lapse rates have been neglected, particularly as proxies may have a seasonal bias in regard to what they preserve. Surface-temperature proxy reconstructions may be biased towards a particular season as a result of critical tolerances (e.g. growing season) (Su et al., 2019), and thermal constraints on mineral formation (Eiler, 2007, 2011; Quade et al., 2007). This issue of seasonal bias is relevant particularly at high altitudes where biological processes slow, or involve dormancy, during the winter months.

Accurate reconstructions of topography are crucial not just for understanding landscape evolution, but also because of the impact the landscape can exert on the climate system and vegetation itself, and these in turn modify lapse rates. The Tibetan region in particular has seen a large body of paleoaltimetry work, some of which includes the application of thermal lapse rates to reconstruct the landscape (e.g. DeCelles et al. (2011); Liu et al. (2016); Rowley and Currie (2006); Spicer et al. (2020b); Su et al. (2019)). This, and the use of isotopic lapse rates, has resulted in a variety of configurations being proposed for the Tibetan region during the Paleogene, including a 'high and dry' plateau (DeCelles et al., 2007; Rowley and Currie, 2006), a more complex configuration where a low valley existed in between two mountain chains (Su et al., 2019), to no significant elevated Paleogene topography at all (Deng et al., 2019; Molnar, 2005). Often modern lapse rates, explicitly or implied, have been used to quantify or reject individual reconstructions, however their ability to accurately reconstruct topography remains uncertain, particularly when multiple lapse rate options are available (Su et al., 2019).

The choice of an inappropriate lapse rate may have far reaching implications. For instance, a monsoonal climate will exert an influence on surface, and near surface, radiative fluxes (sensible and latent heat release; e.g. (Acosta and Huber, 2020)) and these will modify the lapse rate towards a Γm profile, whereas a dry/desert region will tend towards a Γd profile. Farnsworth et al. (2019) showed that the East Asian monsoon region went through periods where the monsoon weakened and even failed for millions of years, thus causing changes in both the local Γe and Γt.

Such changes impact moist processes in an airmass (i.e. the difference between a dry-bulb (ambient) and wet-bulb temperature), and these also must be factored into any lapse rate consideration. A wet-bulb temperature is the temperature of an airmass that would result if cooled to saturation. Airmass moisture content will differ from region to region and along the trajectory of an air parcel from source to deposition. The impact of moist processes could modify temperatures profiles and lapse rates, adding uncertainty in lapse rate calculations due to differential latent and sensible heat release from moisture source-to-sink. All this means that employing a modern-day standard global mean annual Γe/Γt may be inappropriate for paleoaltimetry studies and will lead to erroneous elevation reconstructions.

Table 1
List of experiments and imposed perturbations to the boundary conditions in this study. Topographic realisations are shown in Fig. 1.

Scenario	Expt. Name	Stage	pCO_2 (ppm)	Gangdese highland	Qiangtang highland	Valley inclusion
Pre-industrial	texpa	Modern	280	-	-	-
Scenario 1 – "control"	teveb	Lutetian	840	~3000 m	~4000 m	No
Scenario 2 – Valley	teved	Lutetian	840	4500 m	4000 m	1500 m
Scenario 3 – High plateau	tevef	Lutetian	840	4500 m	4000 m	No
Scenario 4 – Low Gangdese	teveh	Lutetian	840	1500 m	4000 m	No
Scenario 5 – Low plateau	tevej	Lutetian	840	2000 m	2000 m	No
Scenario 6 – 4xCO2	teuyc	Lutetian	1120	~3000 m	~4000 m	No
Scenario 7 – 2xCO2	teuyC	Lutetian	560	~3000 m	~4000 m	No

General Circulation Models (GCMs), used in conjunction with proxy evidence, offer the opportunity to help constrain some spatial and temporal sources of uncertainty in the application of paleo-thermal lapse rates (Feng and Poulsen, 2016). Here we investigate the application of GCMs in paleoaltimetry for the Pre-industrial and for the Eocene, a warm climate of the past (specifically the Lutetian, ~45 millions of years ago (Ma)), to help pinpoint sources of uncertainty and provide a more structured approach to thermal lapse rate application in paleoaltimetry.

We use a series of paleogeographic reconstructions from the Eocene to test how similar (or not) Eocene lapse rates are to the modern at different spatio-temporal scales, and what impact these have on paleoaltimetry reconstructions. We choose the Eocene as it has been identified as the main interval of orographic development throughout the Tibetan region (Botsyun et al., 2019; Ding et al., 2014; Spicer et al., 2020b; Valdes et al., 2019; Xiong et al., 2020).

2. Methods

To investigate the spatio-temporal determinants of thermal lapse rates we use a coupled Atmosphere-Ocean General Circulation Model (AOGCM) (specifically HadCM3BL-M2.1aD, (Valdes et al., 2017), with time-specific boundary conditions for the Pre-industrial and Lutetian (~45 Ma).

For the Pre-industrial, we utilise modern-day observed geographies and a modern-day orbital configuration. Atmospheric CO_2 concentrations are prescribed at 280 ppm, and solar luminosity specified at 1365 W/m^2. For the Lutetian time period GCM paleogeographic boundary conditions (topography, bathymetry, ice sheets) were constructed by Getech Plc. (see Lunt et al., 2016 for further details). Atmospheric CO_2 concentrations are prescribed at 840 ppm (Foster et al., 2017), solar luminosity calculated at 1359.83 W/m^2 (Gough, 1981), and again we use a modern-day orbital configuration.

The paleogeographies were produced at an original resolution of 0.5° × 0.5° (longitude and latitude), and from these we generated GCM-resolution (3.75° × 2.5°) land-sea mask, topography and bathymetry, and the sub-grid scale orographic variables required by the model. This spatial resolution is comparable to the coarse topography so far derived from sparse proxy data, and therefor allows broad-scale comparison with existing literature. To move to a higher resolution at this time would involve some degree of landscape invention, that could itself be a cause of uncertainty in model/proxy comparison. GCMs of this resolution have been used to reconstruct regional scale features and trends from the fossil record, for instance the evolution of the East Asian Summer Monsoon (Farnsworth et al., 2019).

A 10,422-year control simulation for the Lutetian was performed to allow the model to reach a steady state in both the atmosphere and deep ocean, with no energy imbalance at the top of the atmosphere. Additionally, we changed the ozone distribution in the model. In the normal Pre-industrial simulation of HadCM3BL, the ozone distribution is prescribed as a static latitude-pressure-time distribution. However, in warmer climates of the past the tropopause rises, meaning stratospheric ozone penetrates into the troposphere (Lorenz and DeWeaver, 2007), which means it is unphysical to prescribe a Pre-industrial tropopause height to past time periods. We therefore replace the ozone distribution with a simple dynamic approach (Smith et al., 2008) in which ozone is coupled to the model tropopause height with constant values for the troposphere (0.02 ppm), tropopause (0.2 ppm) and stratosphere (5.5 ppm). This change makes negligible difference to the global mean surface temperature, but does have a small impact on stratospheric temperatures and winds.

From the Lutetian control simulation we create four sensitivity simulations where the prescribed topography is modified significantly based on various proposed reconstructions of Tibetan topography (Spicer et al., 2020b) (Table 1; Fig. 1). Scenario 1 is the 'default' Getech Plc. reconstruction of Tibet based on both open source and industry records (Lunt et al., 2016). Scenario 2 is a configuration proposed by (Ding et al., 2014) and Su et al. (2019) where Tibet is composed of two east-west trending mountain chains with a low valley in between (Su et al., 2019). Scenario 3 suggests a high 4 km Tibetan plateau having formed in the Eocene (DeCelles et al., 2007; Rowley and Currie, 2006). Scenario 4 implies that Tibet as a plateau had not risen to any great extent in the Eocene and that its elevation was a more recent phenomenon (in the Miocene-Pliocene) (e.g. Molnar (2005) and Deng et al. (2019)). Scenario 5 evokes a low 2 km Tibetan Plateau starting to rise in the Eocene (Botsyun et al., 2019). All scenarios will have an impact on local and regional climate and, in turn, lapse rates. Here we will test whether these configurations can be accurately reconstructed using current paleoelevation thermal lapse-rate techniques, with known surface temperatures at Mean Sea Level (msl) and at height using modern and Eocene lapse rate expressions. We also explore what biases, if any, exist.

Specifically, the height and spatial extent of the Gangdese and Qiangtang uplands is varied for the Tibetan region (Table 1). Fig. 1 shows the four new topographic realisations and latitudinal cross sections through the Tibetan region for each of the scenarios. Each scenario is run for 500 model years with a mean climate pro-

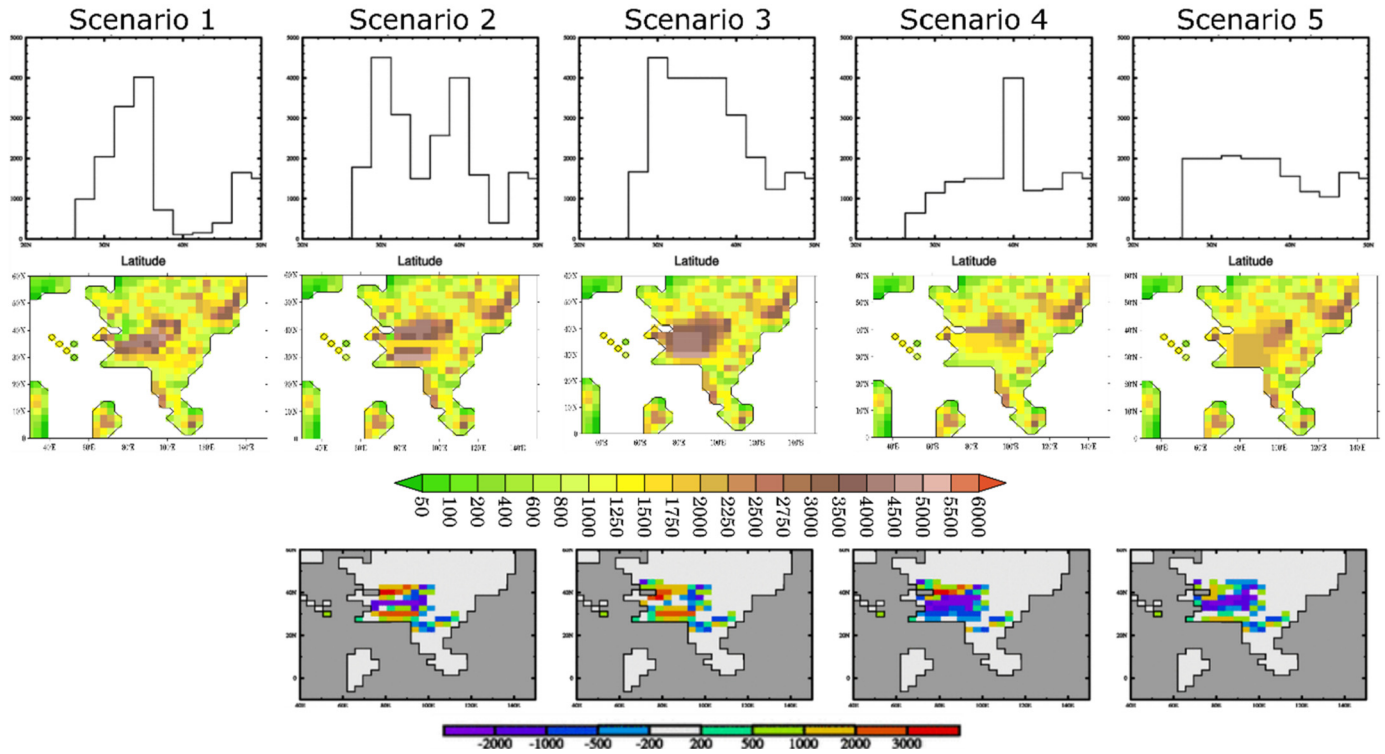

Fig. 1. Orographic reconstructions for the "control" (left column) and the 4 sensitivity simulations. The middle row indicates the elevations (at model resolution) for the alternative paleoelevations of Tibet (Table 1). The bottom row shows the difference between each scenario and scenario 1 (the "control"; m). The top row shows a cross-section at 80°E, illustrating the different behaviours of each terrain for each scenario. All plots show the resolution of the input files to the GCM.

duced from the last 100 years of each simulation. Further, we test the impact of variable atmospheric CO_2 on lapse rates by comparing two similar simulations (Table 1; scenarios 6 & 7), where the CO_2 value is set to 4x (1120 ppm) and 2x (560 ppm) Pre-industrial CO_2 with both simulations running for 10,422 model years to achieve steady state in both the deep ocean and the atmosphere.

We apply the four different expressions of lapse rates for each time period and topographic scenario to predict global land elevation based on the model temperatures to ascertain:

i) if HadCM3L-derived lapse rates can predict accurately the prescribed model height,

ii) which lapse rate expression is the most appropriate predictor of surface height, and

iii) how important spatio-temporal variations are in lapse rates for paleoaltitude estimation.

Both Γd and Γm are theoretical rates. The modern standard for Γd is 9.8 °C/km and can be calculated using:

$$\Gamma \mathrm{d} = -\frac{\partial T}{\partial Z} = \frac{g \cdot MW}{R + Cv \cdot MW} \tag{1}$$

where g is the acceleration due to gravity (9.81 m/sec^2), MW is the Molecular Weight of dry air (28.96x10-3 kg/mol), R is the gas constant (8.3145 J/mol), Cv is the heat capacity, with the quantity $(Cv \cdot MW)$ the heat capacity expressed in units of energy per mole per degree.

The modern standard saturated adiabatic lapse rate (Γm) of approximately ~4–9 °C/km (6 °C/km), is calculated using:

$$\Gamma \mathrm{m} = g \frac{1 + \frac{L_v r_v}{RT}}{C_{pd} \frac{L_v^2 r_v \varepsilon}{RT^2}}, \tag{2}$$

where g is gravitational acceleration, C_{pd} is the specific heat at constant pressure of dry air, r_v is the mixing ratio of water vapour, L_v is the latent heat of vapourisation, R is the gas constant for dry air, ε is the ratio of the gas constants for dry air and water vapour, and T is temperature.

In the free atmosphere the Environmental lapse rate (Γe) will normally fall in between the Γd and Γm, with the modern standard Γe being given as 6.5 °C/km up to 11 km in the atmosphere. Typically, an Γe lapse rate is calculated within the troposphere, the upper bound of which, the tropopause, has a height of between 6–11 km today. For this study we will calculate the free-air Γe lapse rate between two standard pressure levels (500-600 hPa; T_1 and T_2 in eq. (3)), which means it is free from the direct effects of surface processes in the model. However, as proxies are sensing the local climate as well as surface processes, the use of a terrestrial lapse rate (Γt) hypothetically should give the most accurate expression of the change in temperature with surface elevation. Γe and Γt are calculated as follows:

$$\Gamma \mathrm{e} = \frac{T_1 - T_2}{Z_2 - Z_1} \tag{3}$$

$$\Gamma \mathrm{t} = \frac{T_{1(surf)} - T_{2(surf)}}{Z_{2(surf)} - Z_{1(surf)}} \tag{4}$$

Where $T_{1\,(surf)}$ and $T_{2\,(surf)}$ are the model mean monthly 1.5 m surface air temperature (K) at two different land-surface points ($T_{2(surf)}$ at the higher elevation) and $Z_{1(surf)}$ and $Z_{2(surf)}$ are known elevations (m) at two different land-surface points ($Z_{2(surf)}$ at the higher elevation). A modern 'standard' Γt of 5.5 °C/km (Axelrod and Bailey, 1976) is based on 88 weather stations in the United States (with an additional three which were international: Carpathians, Kenya and Brazil). We calculate Γt per grid point by finding the highest elevated grid-point surrounding Γt ($n_{i,j}$) to obtain the differential (eq. (4)).

Table 2
Annual and seasonal Pre-industrial and Lutetian (Scenario 2) simulations for the Environmental Lapse rate (Γe), land only Environmental Lapse rate (Γe_t) and Terrestrial Lapse rate (Γt) as a global mean, and Northern Hemisphere (NH) and Southern Hemisphere (SH) equivalents. 'TIBET' is here described as 25°N-40°N, 75°E-97.5°E for the Pre-Industrial and 20°N-40°N, 63.75°E-93.75°E for the Lutetian.

	Pre-industrial lapse rates (°C/km)											
	Γe				Γe_t				Γ t			
	Global	NH	SH	TIBET	Global	NH	SH	TIBET	Global	NH	SH	TIBET
Annual	6.23	6.17	6.26	6.72	6.41	6.38	6.42	6.72	4.90	4.99	4.71	6.06
DJF	6.16	6.21	6.09	6.68	6.36	6.35	6.36	6.68	5.41	5.97	3.74	5.39
MAM	6.22	6.29	6.13	6.71	6.41	6.54	6.22	6.71	4.45	4.00	5.93	7.03
JJA	6.31	6.13	6.46	6.41	6.47	6.40	6.53	6.41	3.98	3.33	6.10	6.42
SON	6.23	6.07	6.46	6.72	6.40	6.25	6.57	6.72	5.77	6.64	3.07	5.39
	Lutetian lapse rates (°C/km)											
	Γe				Γe_t				Γt			
	Global	NH	SH	TIBET	Global	NH	SH	TIBET	Global	NH	SH	TIBET
Annual	5.95	5.88	6.02	7.14	6.21	6.06	6.36	7.14	3.57	3.13	4.35	4.69
DJF	5.84	5.88	5.79	6.45	6.00	5.91	6.08	6.45	3.66	5.91	-0.16	5.52
MAM	5.95	6.03	5.85	7.14	6.32	6.29	6.19	7.14	3.51	1.67	6.72	4.98
JJA	6.03	5.83	6.22	7.72	6.28	6.12	6.54	7.72	2.23	-0.95	7.75	3.76
SON	6.00	5.76	6.23	7.18	6.21	5.93	6.67	7.18	4.88	5.87	3.15	4.50

$$\Gamma t\left(n_{i,j}\right) = \max_{T_{(surf)}, Z_{(surf)}}(-1 \leq i, j \leq +1) \quad (5)$$

Where $T_{(surf)}$ and $Z_{(surf)}$ are the 1.5 m surface air temperature and orographic height respectively. We only calculate Γt where δZ is ≥500 m. This method calculates a consistent differential over 5° of latitude (two model grid-cell widths) minimising the impact of incident solar radiation as a function of latitude on surface temperature.

For a specific lapse rate expression (γ) and two surface temperature (T; °C) reconstructions the difference in elevation (δZ) is:

$$\delta Z = \frac{(T_1 - T_2)}{\gamma} \quad (6)$$

where T_1 is the lowest elevation temperature datum and T_2 is temperature at height (for Γt and δZ this is calculated at the land surface height (e.g. $T_{1(surf)}$ & $T_{2(surf)}$) so that the absolute elevation can be estimated.

In this study we take the model surface temperatures as the 'truth' to see which lapse rate expression shows skill in reconstructing the prescribed model terrestrial elevation.

Airmasses will both cool and warm as a result of moist processes (exothermic and endothermic reactions), which may substantially differ at both msl and the datum at height. Here we derive a wet-bulb temperature (both Stull (2011, eq. 7) and Davies-Jones (2008); T_wStull and T_wD-J respectively) to assess the predictive skill in reproducing the prescribed model topography in the Tibetan region (Fig. 9). A wet-bulb temperature is the temperature of an airmass once cooled to saturation (100% relative humidity) by evaporation of water into it, as opposed to the frequently used ambient 1.5 m air temperature (dry-bulb temperature) in lapse rate calculations. As a rule, as temperature increases (such as a change in height or pressure), the ability to hold more water also increases and relative humidity decreases. When relative humidity increases temperature decreases. Using wet-bulb temperatures to calculate lapse rates can allow a more consistent comparison between different locations.

To explain the impact of moist processes on lapse rates we calculate two expressions of wet-bulb temperatures:

i) wet-bulb temperature calculated from Stull (2011) (eq. (7)), and equivalent lapses rates (eq. (4) & (5)), and assess its predictive skill for paleoelevation (eq. (7)). The first expression is calculated as:

$$T_w\text{Stull} = T \times \text{atan}[0.151977 \times (\text{RH\%} + 8.313659)^{1/2}] + \text{atan}(T + \text{RH\%}) - \text{atan}(\text{RH\%} - 1.676331) + 0.00391838 \times (\text{RH\%})^{3/2} \times \text{atan}(0.023101 \times \text{RH\%}) - 4.686035. \quad (7)$$

Where T is temperature (°C) and RH% is the relative humidity (%).

ii) The second expression of wet-bulb temperature (T_wD-J) is derived from a more accurate computation (Sherwood and Huber, 2010) from Davies-Jones (2008; their eq. 3.8) with equivalent potential temperature (θ_E) calculated from Bolton (1980; their eq. 38). Because T_wStull is calibrated for the modern day it may not be applicable to past warm time periods, and therefor we show a comparison between both T_wStull and T_wD-J to evaluate their respective skill in reproducing both modern and past Tibetan topographies.

We then apply the wet-bulb (T_wStull and T_wD-J) derived temperatures into Eq. (2), Eq. (5) and Eq. (6) ($T_{1(surf)}$ and $T_{2(surf)}$) to determine elevation differences.

3. Results

3.1. Pre-industrial model lapse rate evaluation:

Our Pre-industrial simulation reproduces a global average Γe of 6.2 °C/km and a Γe_t of 6.4 °C/km (land only environmental lapse rate), closely matching the observed values from Barry and Chorley (1987) of 6.5 °C/km. This shows that the model has some skill at reproducing observed values. The ratio $\Gamma e/\Gamma e_t$ is not spatially constant and will vary with height, season and location. For instance, Γe can vary with height as a global standard between ~5 °C/km in the lowest 2 km above sea level, to ~6 °C/km between 4–5 km, and ~7 °C/km between 6-8 km (Barry and Chorley, 1987). Our Pre-industrial simulation again shows skill in that with increasing height Γe is 4.7 °C/km, 6.2 °C/km and 6.7 °C/km respectively. Seasonally, there is little variability in the global average Γe and Γe_t when separated hemispherically (Table 2).

In desert regions, we would expect the lapse rate to be near Γd due to a lack of atmospheric moisture content. However, in the model, only during JJA (June-July-August) (Fig. 2) does the modelled Γ in the desert regions of Eurasia and Africa approach this value. HadCM3L Γe is in good agreement with ERA-Interim (1979-1984) reanalysis showing model skill. Comparison with ERA-Interim and NCEP reanalysis (both re-gridded to HadCM3L res-

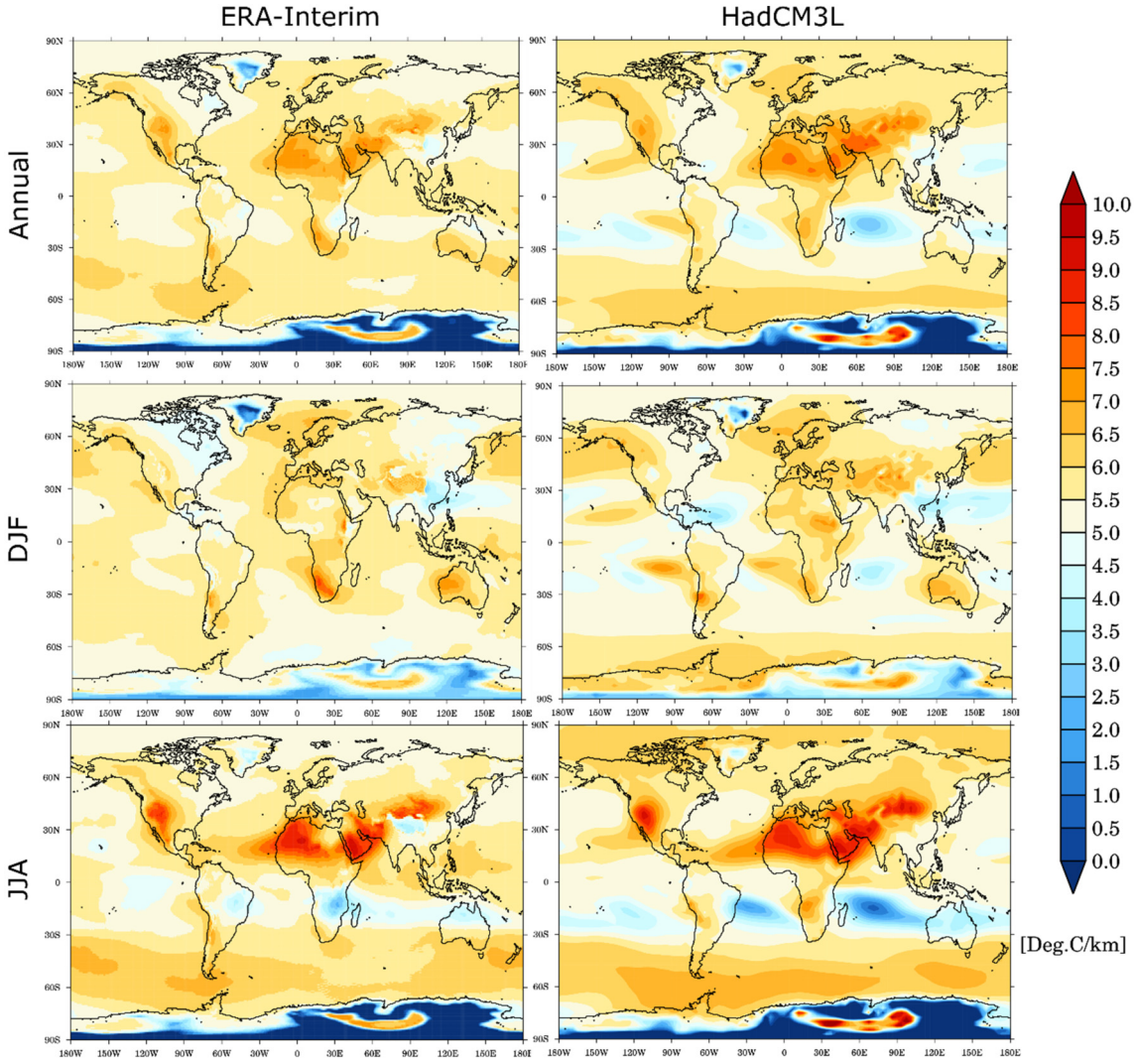

Fig. 2. Comparison of ERA-interim 1979-1984 (left) and HadCM3L (right) Γe calculated between 700-600 hPa for Annual (top row), DJF (middle row), and JJA (bottom row).

olution) (not shown) indicates that model relative humidity at 700 hPa is broadly similar in DJF (December-January-February) and MAM (March-April-may), and even slightly too high (by 10%) in JJA and SON (September-October-November) over desert regions, so the low lapse rate is not due to moisture errors in JJA and SON over desert regions. It might be that moisture is being entrained into the region in the mid-atmosphere. This suggests that during certain seasons some processes are leading to lower model annual Γ (more towards an Γm).

Within continental interiors, we observe a seasonal signal in boreal winter lapse rates that is generally smaller than boreal summer (not shown), and in some cases negative (temperature inversion) due to radiational cooling over snow surfaces as commonly observed throughout much of the year in the lower troposphere of the Arctic and Antarctic.

The simulated Pre-industrial global mean annual Γt of 4.9 °C/km is near the modern observed (1960-1990) values of 5.5 °C/km (Wolfe, 1992) calculated from a combination of north-western United States sites. Table S1 (Supplementary information) comparing a combination of the sites from (Wolfe, 1992) and other similar studies, the observed mean annual Γt is 5.8 °C/km, in good agreement with the equivalent sites in the model of 5.6 °C/km. This suggests that previously accepted global mean "standard" value Γt of 5.5 °C/km, derived from relatively few sites globally, may be an overestimate compared to the whole planetary land surface average Γt in the model (Γt of 4.9 °C/km). Seasonal variations occur during the year with highest lapse rates during the boreal/austral autumn and winter (Table 2).

Locally, observed Γt measurements are highly variable between weather stations within the same mountain chain (Rolland, 2003; Wolfe, 1992). This can be a function of local climate and when that variation is at a finer scale than model spatial resolution it complicates comparisons between the model and the observations. However, along the windward trajectory of the Rocky Mountains, simulated Γt does show some agreement (Table S1) with observed Γt (Wolfe, 1992; his table 4 & 13 therein). It should be noted that slope, aspect, and vegetation cover can all have an impact on the 1.5 m surface temperature. A more comprehensive analysis incorporating additional geographic locations over time is required to obtain a more complete observational dataset to evaluate Γt against the model.

The application of the Deming regression (Wu and Yu, 2018), which provides an accurate skill score encompassing observational and model standard error, shows that annual Γt from the Pre-industrial simulation correlates moderately (r =0.75) with observations (Table S1). However, for warm-month mean (WMM) and cold-month mean (CMM) Γt shows either weak or no agreement (r=0.57 and r=0.46 respectively). Moreover, there is considerable spatial variability in the predictive skill of the model. For example, if only the Asian region sites are chosen then Annual (r =0.87) and

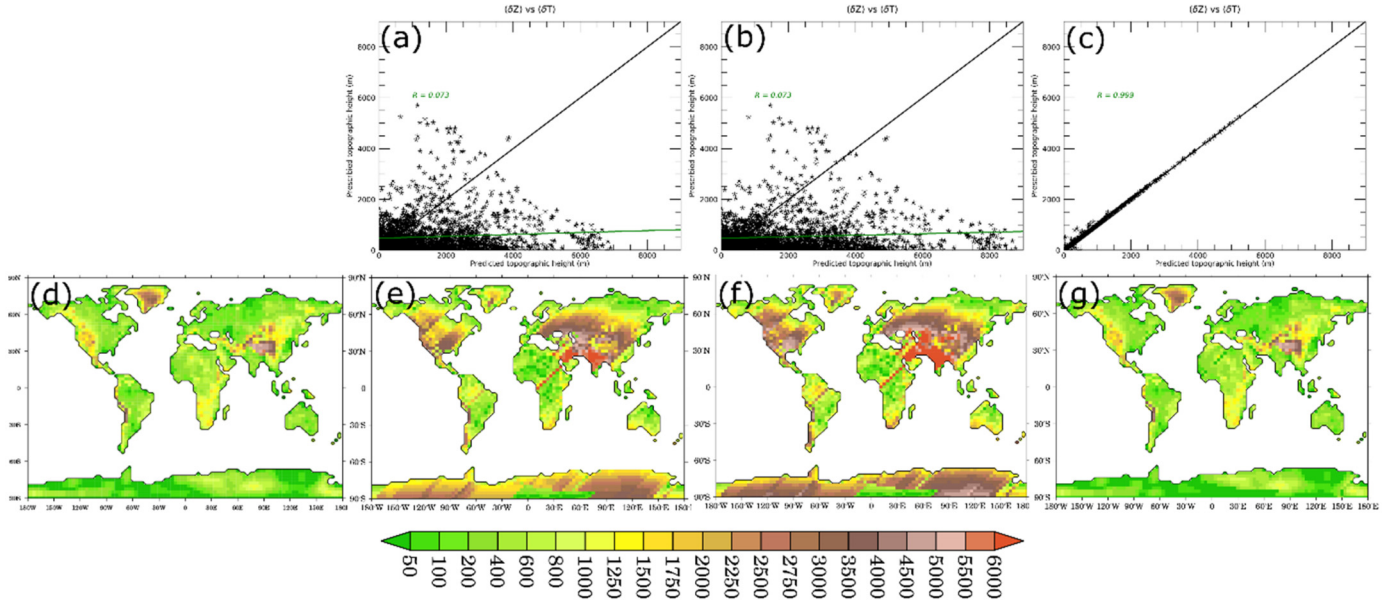

Fig. 3. Correlation between Pre-industrial elevation (using the back-trajectory model to find msl moisture source) against the prescribed model elevation using annual global mean Γe (a), global mean Γt (b) and elevated-msl source Γt_{origin} (c). Bottom row shows the corresponding topographic (m) prediction against the prescribed model topography (d) shown for global mean Γe (e), global mean Γt (f) and local lapse rates with known msl airmass origin and at height surface temperature (g). Green line depicts line of best fit.

CMM (r =1.00) scores are improved, but not the WMM (r =0.43). However, the sample size is small and requires increasing to improve the robustness of this result. Reduced skill in WMM/CMM Γt in certain regions suggests that HadCM3L is producing a seasonal range that maybe outside the envelope of modern observations. However, ERA-40 reanalysis and HadCM3L seasonal ranges are broadly comparable, suggesting similarity between global and regional scales (Gasson et al., 2014). Unfortunately, a site-specific comparison of *in-situ* observed annual, WMM and CMM surface temperatures is not possible because seasonal values were not reported in Meyer (1992) nor Wolfe (1992) (Table S1). Because local weather and climatic conditions can vary on different temporal and spatial scales, it is likely that local seasonal variations are not being captured at the model resolution. More lapse rate (Γe and Γt) observations are required over large spatial regions and globally to ascertain if weather and climate prediction models are adequately capturing spatio-temporal variations in lapse rates. Nonetheless, this is less problematic on an annualised basis where local seasonal variations in surface temperature are homogenised.

3.2. Pre-industrial topographic prediction evaluation:

The Pre-industrial simulation shows reasonable skill at reproducing observed global and regional lapse rates ($\Gamma e/\Gamma e_t/\Gamma\tau$; Table S1). Here we use the model to assess its predictive skill at reproducing the prescribed topography. We use a back-trajectory model that follows the climatological wind trajectory of the airmass (at 850 hPa), on a monthly basis, from the elevated topographic grid-point back to its msl origin to calculate the change in temperature and therefore derive specific $\Gamma\tau$. We then apply this model grid-point specific $\Gamma\tau$ and global $\Gamma\tau/\Gamma e/\Gamma e_t$ to calculate the elevation at each grid-point. This tests the predictive skill of reproducing the model prescribed topography for each lapse rate expression.

Reconstructing topography using a global mean $\Gamma\tau//\Gamma e_t$ shows no predictive skill (Fig. 3a, b), because it produces an unrealistic topographic surface in both spatial extent and height (Fig. 3 e,f) when compared to the prescribed topography. As a 'sanity check', we calculate the local terrestrial lapse rate (Γt_{origin}) between two sites, one at the msl origin and the other at height. As expected, this reproduces the prescribed model topography (Fig. 3c, g (compare with d)).

Land-surface temperatures respond differently to incident solar radiation as a result of dissimilar dynamic (e.g. topographic barriers, aspect, slope) and thermodynamic (e.g. vegetation albedo, soil properties, proximity to water bodies, atmospheric circulation and entrained constituents) processes. Even at the same latitude, and with no change in elevation, surface temperature can differ significantly from location to location, which means that a global standard lapse rate cannot be used to reliably reconstruct the topographic surface (Fig. 7). This is a result of low land surfaces, especially in continental interiors, having a large temperature gradient that is not associated with a change in altitude, but differences in regional atmospheric circulation as a function of the distance of an air mass from its msl origin. If elevated surfaces globally are masked out below 2 km, 3 km, 4 km and 5 km (Fig. 4) respectively, all global mean annual lapse rate expressions show no skill in representing the specific elevation as a function of the change in temperature from msl.

In the case of the Tibetan region alone, and with the topographic surface masked out below 2 km, again all global mean lapse rate expressions fail to show adequate skill in reconstructing the actual change in elevation from msl (Fig. 4, 8). However, due to the large seasonal range in temperature (~20-30 °C) in the Tibetan region, a marked seasonal component to lapse rates might be exploited to better represent higher elevations. MAM and JJA mean global lapse rates show an improved, albeit not perfect, fit to elevation as a function of temperature change with height at 2 km (Fig. 7) compared to the global mean annual lapse rate. MAM shows the most skill (r >0.8) for both Γe and Γt (Fig. 7), but with a positive bias in the reconstructed elevation compared to the prescribed height, whereas DJF, JJA and SON show no skill in reproducing prescribed model elevation. There is a small discrepancy for a couple of model grid-boxes in the back-trajectory model where the back tracking of the air parcel in the model is not able to find its msl, so producing anomalous tracks seen in Fig. 7 (e,f). This is a result of internal wind vortices at 850mb whereby the air parcel is advected vertically to a pressure level that allows it to es-

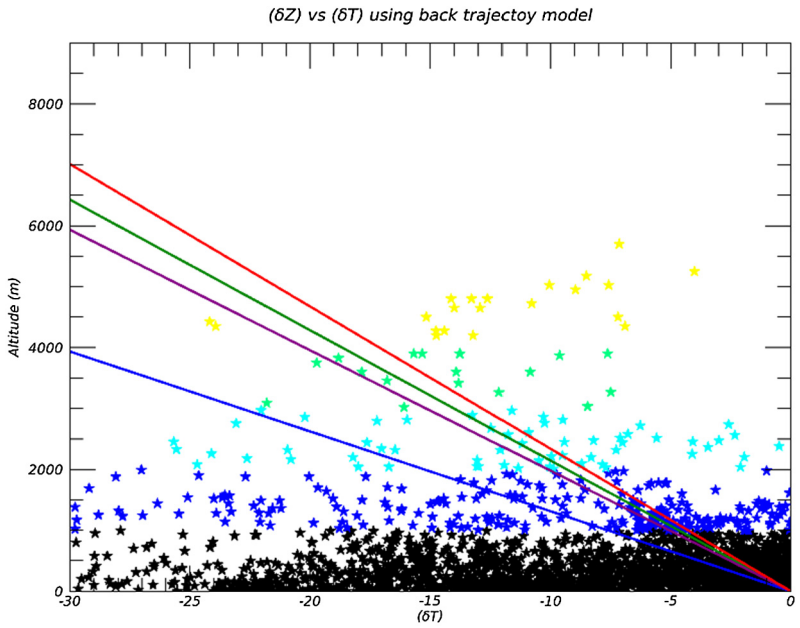

Fig. 4. Global mean annual thermal lapse rate vs. topographic height. Different global mean lapse rates (dT/dZ) calculated from grid-point at height and grid-point at msl in the back-trajectory model) with Γd (blue line); Γm (green line), Γe (purple line), Γt (red line) for each land grid-point (a), every land grid-point with an elevation <1 km (black stars), >1 km and <2 km (dark blue stars), >2 km and <3 km (light blue stars), >3 km and <4 km (Green stars) and >5 km (yellow stars).

Table 3
Annual and seasonal Lutetian simulations (all scenarios) Environmental Lapse rate (Γe) and Terrestrial Lapse rate (Γt) over 'TIBET' (20°N-40°N, 63.75°E-93.75°).

	Lutetian lapse rates (°C/km) in Tibet									
	Γe					Γ t				
	Scn.1	Scn.2	Scn.3	Scn.4	Scn.5	Scn.1	Scn.2	Scn.3	Scn.4	Scn.5
Annual	6.98	7.13	7.14	6.95	7.08	4.56	4.69	4.38	3.70	3.82
DJF	6.36	6.45	6.66	6.11	6.01	5.57	5.52	5.14	6.76	6.04
MAM	6.85	7.14	6.98	6.89	7.04	4.98	4.98	4.63	3.72	4.15
JJA	7.80	7.72	7.66	7.99	8.25	3.18	3.76	3.61	0.94	1.47
SON	6.86	7.18	7.24	6.75	6.96	4.49	4.50	4.13	3.37	3.61

cape these internal vortices to a msl source. Reconstructions where this track is visible should be disregarded.

3.3. Middle Eocene (Lutetian) topography prediction evaluation:

Here we apply the same framework to the Lutetian (∼45 Ma) for five different topographic realisations of the Tibetan region (Fig. 1). We also investigate the impact of variable pCO_2 for scenario one at 2x and 4x Pre-industrial pCO_2 (280 ppm) pCO_2. A comparison between the Pre-industrial simulation (Table 2) and Lutetian simulations (Table 3) indicates that model lapse rates in the Lutetian were consistently lower Γe, Γe_t and Γt. However, this is dependent on the topographic configuration. Table 3 shows that regionally the 5 different Tibetan scenarios produce widely varying regional terrestrial lapse rates, especially when compared to the Pre-industrial simulation, highlighting the inappropriateness of the use of modern-day lapse rates for past time periods. Global annual mean Lutetian Γe, Γe_t, and Γt are respectively 4.5%, 3.1%, and 27.1% lower than the Pre-industrial.

In all five topographic scenarios (Figs. 6 & 8) global mean Γe and Γt show no skill in reproducing the elevation and topographic extent of Tibet. In both cases, low-lying regions are erroneously elevated to heights in excess of 5 km. This erroneous overestimation is also the case for the valley (prescribed valley low at 1.5 km) in scenario 2 where a >5 km height was predicted. This showcases the erroneous impact of using global mean lapse rates. Conversely, the predicted height of the Gangdese (prescribed 4.5 km) and Qiangtang (prescribed 4 km) mountain ranges in scenario 2 is underestimated by ∼2 km (Figs. 6 & 8). This indicates that annualised lapse rate predicted topography is anticorrelated to that of the actual topographic height for elevations greater than 2 km.

Interestingly the topographic predictive skill for global mean Γe and Γt in the Tibetan region is also highly dependent on seasonal variation in climate. For global mean Γe and Γt, MAM shows the highest predictive skill while DJF, JJA and SON show no skill, or are anticorrelated (Fig. 7). For MAM, low-lying topography (2-3 km) is underestimated, giving lower elevations compared to the prescribed model elevation (Fig. 5 & 8). This negative elevation bias is present for all predicted topographic scenarios when using a seasonal MAM global mean Γe and Γt. MAM global mean Γt however produces near-equivalent predicted elevations in agreement with the prescribed model elevations between 3-5 km (Fig. 6). This indicates that global mean Γts have greater predictive skill for higher mountain elevations compared to the global mean Γe, which tends to underestimate elevation by ∼1-2 km.

Often multiple regional msl proxy-surface temperature data (T_1) are not available to calculate the change in temperatures with height (Eq. (6)). Depending on the msl location the derived heights may vary based on different msl temperature baselines. Applying local Γt to 4 different msl surface locations of T_1 (star symbols denoted in Fig. 8), three within the Tibetan region and one site chosen in N. America (30°N, -86°E) at a similar latitude, is marginal. We choose to explore a N. American site here on the

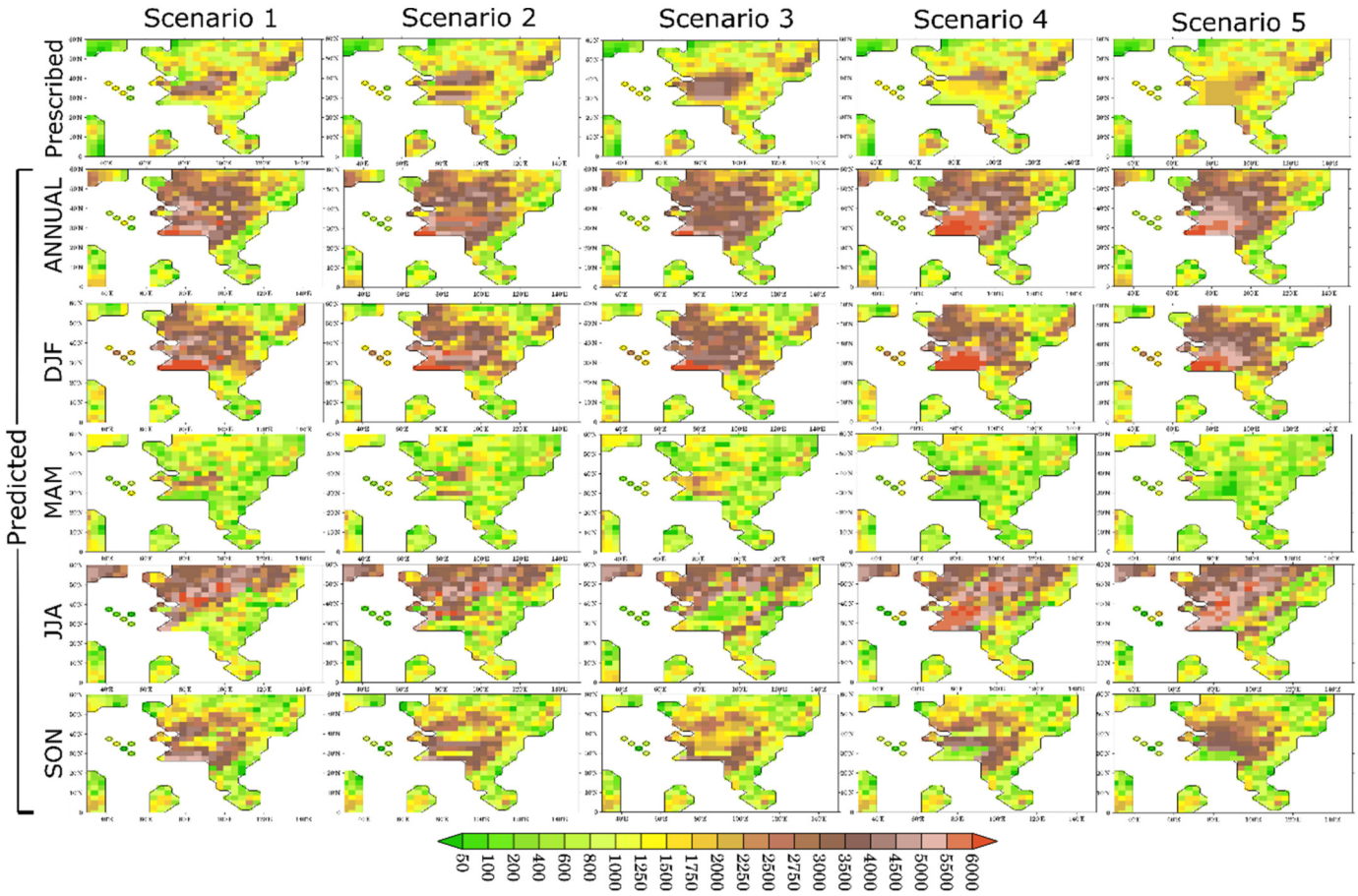

Fig. 5. Prescribed Tibetan model topography for Lutetian scenarios 1-5. Annual, DJF, MAM, JJA and SON global mean environmental lapse rate (Γe) predicted Tibetan topography for scenarios 1-5.

basis that msl proxy-sites, particularly in deep time, can be sparse with little recourse but to utilise sites that geographically distant. However, it may be that distant sites at the same latitude which receive similar levels of incident solar radiation may be used as a surrogate when no geographically close sites are available. Each T_1 location reproduces the spatial topography of the Tibetan region, however the heights can be overestimated or underestimated depending on the site versus the prescribed topography (top row, Fig. 8).

The influence of increasing pCO_2 in the Lutetian from 560 ppm to 1120 ppm (using scenario 1 only) results in a 0.1 – 0.5 °C/km decrease in each of the global annual mean thermal lapse rate expressions.

The disparity between seasonal and annual lapse rates (both Γe and Γt) and higher predictive skill in MAM suggests airmass modification along its trajectory, becoming less representative of its source region.

Fig. 9 indicates increased predictive skill for annual and seasonal wet-bulb lapse rate predicted topography in the Tibetan region over dry-bulb derived lapse rates. The more appropriate Davies-Jones (2008) wet-bulb formulation shows greater skill over that of the Stull (2011) wet-bulb solution, regardless of seasonal or annual lapse rates and predicts a topography that is very close to the prescribed topography (see Fig. 10). Both environmental and terrestrial wet-bulb derived lapse rate both show equally good skill regardless of state dependence such as global paleogeography and $pCO2$ (Fig. 9–10 and Figure S1). This highlights that moist processes have an appreciable impact on lapse rates, and thus paleoelevation reconstructions.

4. Discussion

The Clausius-Clapeyron relation shows that the moisture holding capacity of the atmosphere increases by ∼7% per 1 °C warming. The Lutetian global and land only mean surface temperatures are 6.5 °C and 5.9 °C warmer than the Pre-industrial simulation. The total atmospheric column integrated (grid weighted) specific humidity over land increases by 42.3% from the Pre-industrial to the Lutetian, roughly in line with Clausius-Clapeyron. However, in general, this increase in atmospheric moisture does not move the lapse rates towards a moister adiabatic lapse rate with total column-integrated land relative humidity at similar levels between the Pre-industrial (280 ppm CO_2; 36%) and Eocene (1120 ppm CO_2; 37%) in opposition to that of Zamora et al. (2016), but in agreement with Held and Soden (2006). However, specifically over Asia (25°N-45°N, 70°E-110°E) total column integrated land relative humidity is markedly different (Pre-industrial: 33%, Lutetian: 24%) suggesting that Asia moved towards a drier adiabat in the Eocene. This is consistent with the higher lapse rates in the Tibet region given in Table 3. This is not sensitive to modification of the regional topography in each scenario. More sensitivity studies are required, but this suggests regional state dependence in atmospheric moisture holding capacity.

These simulations have shown that between the Pre-industrial and the Eocene the Γe does not significantly change (Table 2) as a global annual mean, but the Γt does. This is unsurprising considering that there are large changes in topography and subsequent land surface processes between the Pre-industrial and Eocene, indicating that past time periods will have different Γts to those of

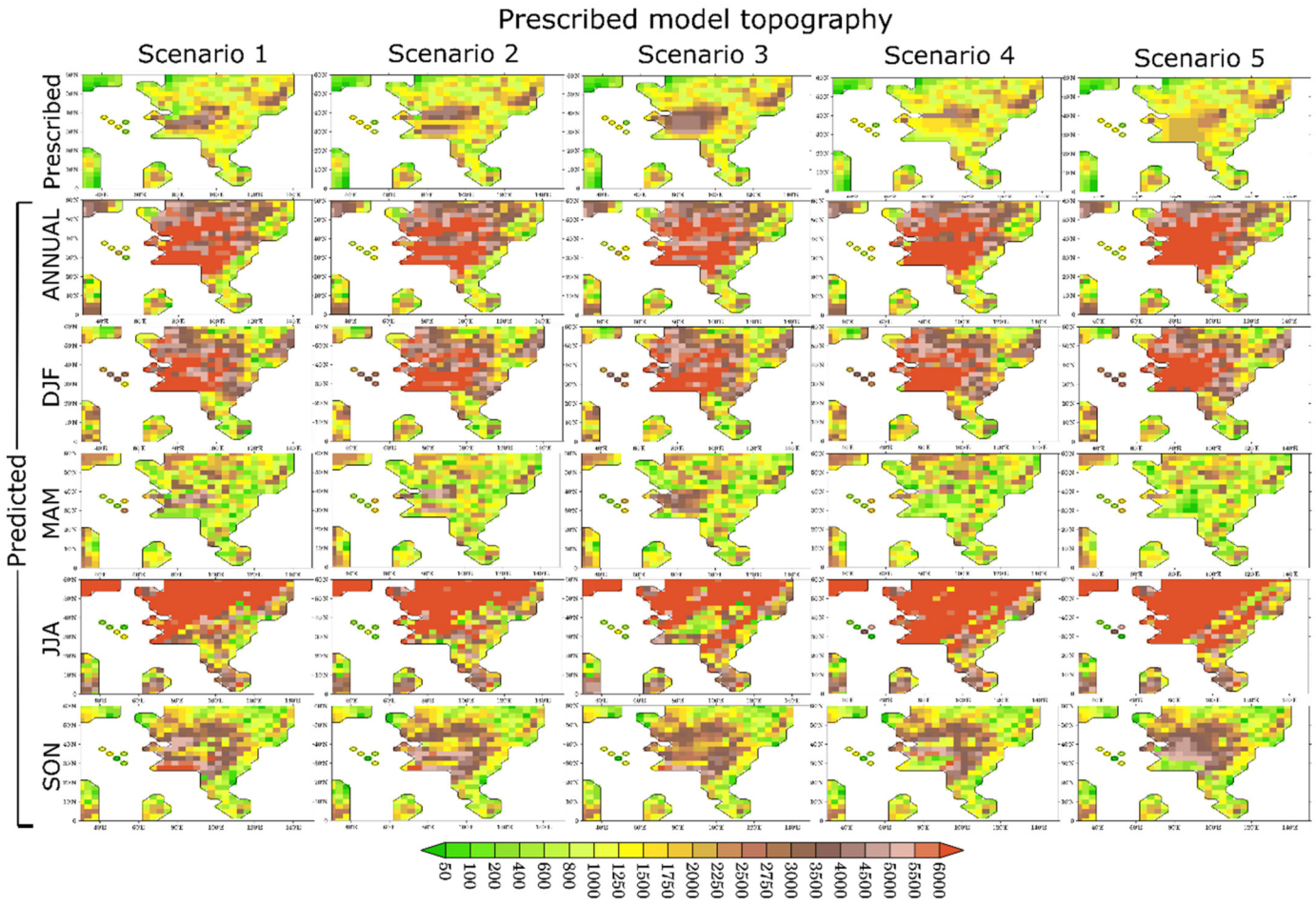

Fig. 6. Prescribed Tibetan model topography for Lutetian scenarios 1-5. Annual, DJF, MAM, JJA and SON global mean terrestrial lapse rate (Γt) predicted Tibetan topography for scenarios 1-5.

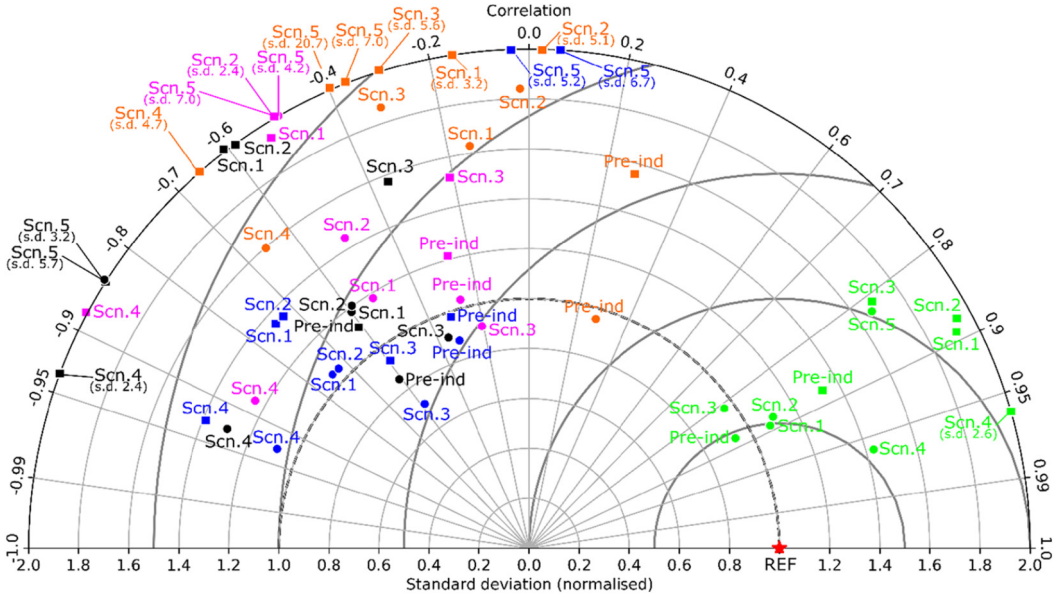

Fig. 7. Taylor diagram depicting the skill of annual (black) and seasonal (DJF (Pink), MAM (Green), JJA (Orange), SON (Blue)) global mean Γe (circle symbol) and Γt (square symbol), derived from 1.5 m surface temperatures, to reconstruct the prescribed Tibetan topography (>2000 m) for each simulation (Pre-industrial, and five Lutetian topography sensitivity studies; Table 1). Each reconstruction is normalised relative to the prescribed reference topography (star symbol). Great predictive skill is shown where colored symbols are positioned closer to the red reference star.

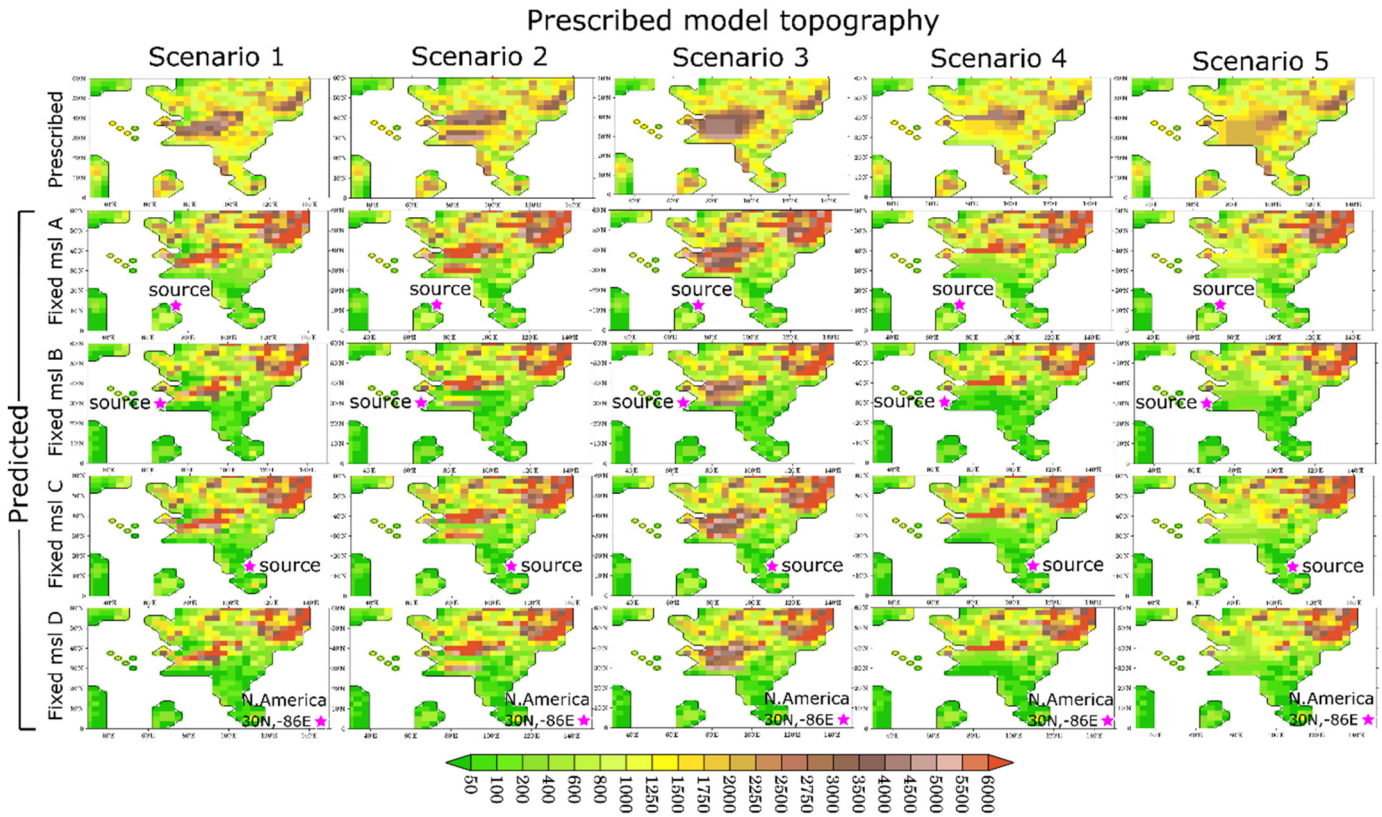

Fig. 8. Prescribed Tibetan model topography for scenarios 1-5 (top row) versus the predicted topography using annual local (derived from a 3x3 grid surrounding each grid square) Γt for each scenario. However, for each row (rows 2-5) the annual msl temperature (T_1 in Eq. (6)) is taken from only one fixed reference location (star symbol) to derive changes in temperature with height over the whole Tibetan region.

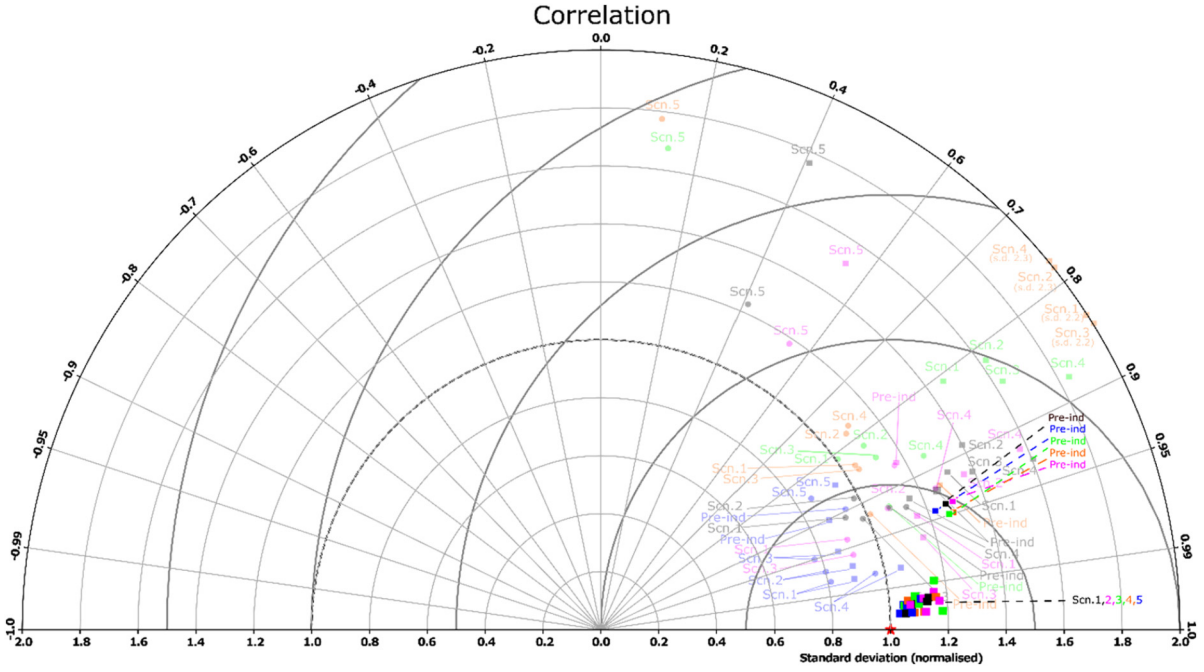

Fig. 9. Taylor diagram depicting the skill of annual (black) and seasonal (DJF (Pink), MAM (Green), JJA (Orange), SON (Blue)) global mean Γe (circle symbol) and Γt (square symbol) derived from 1.5 m wet-bulb surface temperature to reconstruct the prescribed Tibetan topography (>2000 m) for each simulation (Pre-industrial, and five Lutetian topography sensitivity studies; Table 1). Stull derived wet-bulb lapse rates (T_wStull) are shown in the faded symbols and colours. Davies-Jones derived wet-bulb lapse rates (T_wD-J) are shown in unfaded colours. Each reconstruction is normalised relative to the prescribed reference topography (star symbol). The closer a point is to the red star symbol, the greater the predictive skill.

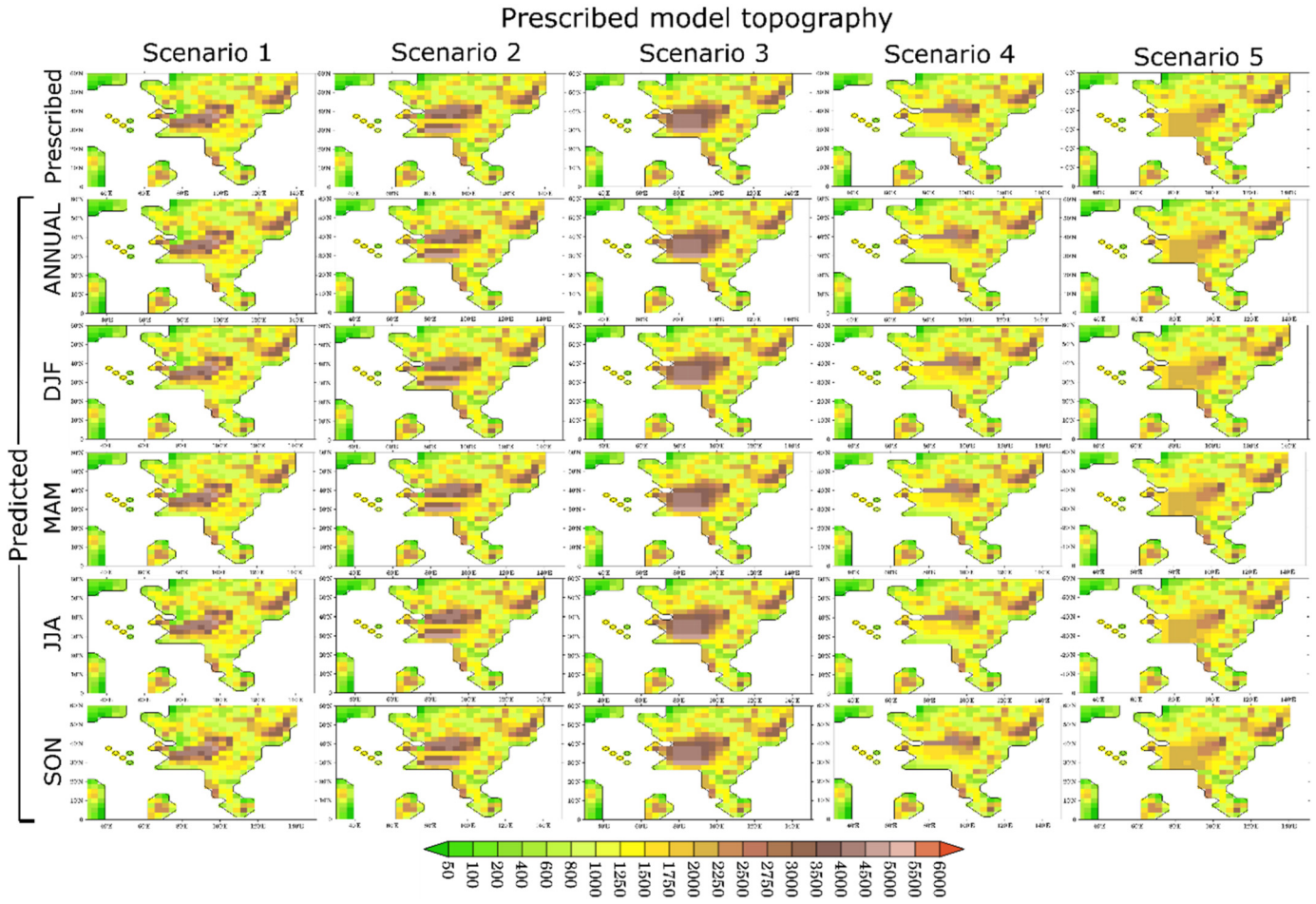

Fig. 10. Prescribed Tibetan model topography for Lutetian scenarios 1-5 (top row). Annual, DJF, MAM, JJA and SON wet-bulb (Davies-Jones method) derived global mean terrestrial lapse rate (Γt_{wb}) predicted Tibetan topography for scenarios 1-5.

the modern. As expected, the use of global annual mean Γ to derive global altitudes shows no skill (Fig. 7). This is most evident in continental interiors where predicted topography is significantly higher than that prescribed in the model, and it results from the large temperature gradients between the interior of continents and the nearest msl point in the back-trajectory model. During transit from its origin the airmass undergoes dynamic and thermodynamic modification as it advects and ceases to be representative of the msl source. Thermal lapse rate paleoaltimetry reconstructions become increasingly unreliable away from coastlines towards continental interiors, and so should be avoided, unless wet-bulb derived lapse rates are used in conjunction with the known msl source temperature datum.

At a local level both observations and the model (Table S1) show that lapse rates can differ significantly as a function of local topographic features and associated climatic conditions. There is also critical disagreement in the global and regional Tibetan mean annual Γe and Γt in both the Pre-industrial (Table 2) and Lutetian (Table 2 & 3) simulations. The use of either lapse rate would lead to highly divergent paleoaltitude reconstructions, with higher predicted altitudes if a Γt were employed. Land surface processes (hydrology, vegetation, slope, aspect, albedo as a function of soil, vegetation, and low cloud) likely play a significant role in buffering land surface temperature change with height (Γt) compared to the equivalent temperature change in the free atmosphere (Γe). Previous studies have often used global annual mean Γe, however, despite surface proxies, such as plants, recording a local climatic signal just above the soil surface, or geochemical proxies recording conditions in soil or aquatic environments. Moreover, even the use of a more appropriate global mean annual Γt would suggest that current paleoaltitude reconstructions could be potentially biased towards higher elevations, in particular in higher latitudes (Fig. 6). This could have a profound impact on the local/regional, and potentially even global climate if such elevations were used to define topographic boundary conditions in models. Likewise, if there was a suspected seasonal component in proxies for either the temperature datum at height, or at msl, this could again result in biases towards higher/lower elevations if using a global annual mean Γt, while Γe shows little seasonal variation.

Using global annual mean lapse rates for paleoaltitude reconstructions cannot be justified. Global mean annual Γe and Γt (for either the Pre-industrial or Eocene), even with precise temperature tie points at height and msl from the back-trajectory model, show no skill in reproducing the prescribed topography in the model (Fig. 7). Only MAM-derived global mean lapse rates (Γe and Γt) show some skill at reproducing the height and spatial extent of the different Lutetian topographic scenarios. MAM-derived Γe generally underestimates the topographic height by 0.5 km-1 km. On inspection of the relative skill of MAM thermal lapse rates it seems that the moisture content of the low elevation airmass at the evaporative source tended to be maintained during its journey to the datum at height, whereas on an annual basis and in other seasons it was not, suggesting moist processes may be exert a critical influence over thermal lapse rates.

Moist processes control airmass moisture content (which will change seasonally). These processes are shown to play a funda-

mental role in the predictive skill of lapse rates. Airmass temperatures with an equivalent relative humidity (e.g. wet-bulb temperature) improve the paleoelevation predictive skill in the model for any topographic configuration of Tibet, for all seasons, and even on an annualised basis (Fig. 7). Of the two wet-bulb calculations performed here, the Davies-Jones (2008) wet-bulb solution is shown to be the most accurate compared to Stull (2011), which is calibrated for a modern climate and so should be avoided in paleoaltimetry. Using a dry-bulb (ambient) temperature will introduce considerable error in reconstructed elevations (Fig. 7), depending on which seasonal or annual lapse rate is used. This applies to both modern and Eocene lapse rates. Whether using a wet-bulb derived lapse rate is a more appropriate for real-world situations is unknown and may be dependent on what the proxy is sensing. For example, a plant proxy might well code wet-bulb temperatures better than dry-bulb because of the sensitivity to evapotranspiration constraints, but this has yet to be tested.

The benefit of seasonal lapse rates may be limited because many proxies tend to be calibrated against mean annual conditions. However, plants often exhibit seasonal growth strategies, particularly at high elevations, meaning a seasonal temperature signal, not an annual one, may be preserved. This is because the rate of photosynthesis and plant growth varies as a function of temperature and precipitation, meaning vegetation is highly sensitive to, and thus adapted to, its immediate climatic environment. Vegetation will develop growth strategies and architectures best suited for seasonally changing regimes. Leaf architectures preserved in the fossil record can be used by techniques, such as the Climate Leaf Analysis Multivariate Program (CLAMP) (Spicer et al., 2020c), to quantitatively reconstruct surface temperature. Fortunately, seasonally deciduous plants have adaptations to increasing spring warmth as leaves expand, meaning that to some extent even the cold month mean temperatures can be derived despite the plant being dormant, although the depth of freezing may be underestimated in extremely cold winters (Spicer et al., 2004). Despite this ability to reconstruct some aspects of past seasonal temperature variation, modern day seasonal lapse rates are not consistent across different past climates, as highlighted by the Lutetian simulations.

Although simulated annual global mean $\Gamma e/\Gamma e_t$ are shown to be not significantly different between the Pre-industrial and Lutetian simulations, global annual mean Γts do differ significantly (compare Table 2 with Table 3). This suggests that paleogeography plays an important role not only in local, but also global, terrestrial lapse rates. For instance, an open large seaway across the Indo-Gangetic region (present in these simulations) will raise the specific humidity in the region compared to the seaway being closed. Uncertainty regarding the age of the closure of this seaway could introduce erroneous lapse rate applications and subsequent topographic reconstruction. More work is needed to understand the paleogeographic role not only for paleoaltimetry, but also in proxy-calibrations (Bai et al., 2018).

We also highlight the impact on predicted paleoelevation if a location at height has multiple downwind msl airmass sources (Fig. 8), with widely different msl source temperatures. When terrestrial wet-bulb (T_wD-J) lapse rates are calculated greater skill is shown (Figure S2) with the exception of a the North American msl reference point. This indicates that sites within a region may be adequate as long as they are sensing a similar climate signal to that of the actual proxy source location. However care should be taken as uncertainty in deconvolving the most relevant msl source location may render any paleoelevation estimate meaningless. This can be partially remedied through model mediation to assess the airmass trajectories to identify the most appropriate msl proxy-temperature datums.

While doubling pCO_2 has a fairly negligible effect on lapse rates (both dry and wet-bulb) in the simulations, changes in paleogeography have a significant effect, suggesting that modern-day observed terrestrial lapse rates cannot be used reliably for the past because they are state dependant.

Paleoclimate simulations offer the opportunity to produce time-specific lapse rates (both dry and wet-bulb derived) for paleoaltimetry studies. Where no msl proxy data are available, well constrained (from proxy-data at a variety of locations) GCM simulations offer the ability to provide a msl-temperature datum from which an elevation can be reconstructed. Critically, paleoclimate models offer the opportunity to calculate time-specific lapse rates that are more representative of the time period at the global, regional and local scale. They also offer a improved understanding of moist processes through the application of wet-bulb temperature derived lapse rates. Currently, there is no other method to produce past climate specific Γt. However, this does require some prior knowledge of the time period, e.g. pCO_2 concentrations, solar luminosity, topography and bathymetry (atmosphere and ocean circulation) and vegetation, all of which can have a significant influence on the paleo-thermodynamics. Because some of these variables (such as paleotopography) are unknown and the subject of the investigation, the simulations need to be iterative.

Further understanding is required to investigate the influence of lapse rate model dependency on predicted lapse rates in warm climates of the past. Improvement in model spatial resolution and complexity, such as models that more accurately capture equable climates of the past, and reproduce shallow latitudinal thermal gradients, may also allow greater accuracy in derived Γt for more complex terrains (Sewall et al., 2000). Over time, past topography can be better quantified iteratively through proxy/model-mediation, allowing for more precise reconstructions of the elevation history of a region.

5. Summary

HadCM3L has shown skill at reproducing various expressions of modern lapse rates against observations both globally and locally. Significantly, modern global annual mean Γe and Γt have been shown to be different between our Pre-Industrial and Lutetian climate model simulations, suggesting that the modern Γe and Γt are not a reliable metric for thermal paleoaltitude studies. Simulated Γt have also been shown to have a sizeable seasonal component that would impact paleoaltitude reconstructions if the relationship between a proxy and seasonal temperature variables is unknown or poorly understood. This needs to be considered when utilising seasonal lapse rates. However, even then, ambient global annual and seasonal mean Γe and Γt have been shown to have little predictive skill in reproducing the prescribed model topography in either the Pre-Industrial, or the suite of Lutetian topographic scenarios presented here. MAM global mean Γts show greater predictive skill for elevations >2 km in terms of the spatial extent and height of the reconstructed topography in the Tibetan region. Conversely, elevations <2 km are inconsistent in their predicted spatial extent and height when compared to the prescribed elevation. We show that differences in airmass moisture content between msl and the datum at height can have a significant impact on derived lapse rates. Only when airmasses with equivalent relative moisture content are considered, regardless of the topographic configuration, does the topographic predictive skill increase (contrast Fig. 7 and 10). Because moisture content can vary throughout the season, the impact can be significant. This uncertainty will likely be exacerbated with greater distances between datum sites, particularly in a latitudinal direction.

With most proxies thought to best represent an annual signal, the use of seasonal lapse rates is likely limited. Model-mediated

lapse rates offer the opportunity to improve the predictive skill for paleolatitude reconstructions by calculating local lapse rates that are more representative of local environmental conditions, but the models require further improvement in respect of spatial resolution (Acosta and Huber, 2020) and cloud physics (Zhu et al., 2019). Importantly, paleoclimate modelling can allow msl temperatures to be calculated where there are no msl source data available to produce a paleoaltitude estimate. However, this does require prior knowledge of the climate system and a rough estimate of the paleotopography. At present, such paleotopographic reconstructions will, in many instances, have been based modern Γ – derived paleoaltimetry. A combined iterative model-data approach may crucially allow greater accuracy for thermal lapse rate-based paleoaltimetry studies improving both reconstructions and simulated climates of the past, in agreement with Feng and Poulsen (2016). Note, however, that where many confounding factors (e.g. unconstrained model boundary conditions if model mediation methodologies are utilised), or unconstrained assumptions (e.g. modern lapse rates, lack of a proxy-msl site) are present, the use of thermal lapse rate reconstructions should be avoided.

Data accessibility

Model data can be accessed here http://www.bridge.bris.ac.uk/resources/simulations.

CRediT authorship contribution statement

Alex Farnsworth: Conceptualization, Investigation, Methodology, Software, Validation, Visualization, Writing – original draft, Writing – review & editing. **Paul J. Valdes:** Software, Validation, Writing – review & editing. **Robert A. Spicer:** Conceptualization, Writing – review & editing. **Lin Ding:** Writing – review & editing. **Caitlyn Witkowski:** Writing – review & editing. **Vittoria Lauretano:** Writing – review & editing. **Tao Su:** Writing – review & editing. **Shufeng Li:** Writing – review & editing. **Shihu Li:** Writing – review & editing. **Zhekun Zhou:** Writing – review & editing.

Declaration of competing interest

The authors declare that they have no known competing financial interests or personal relationships that could have appeared to influence the work reported in this paper.

Acknowledgements

Author Contributions are as follows. A.F. carried out the simulations, analysis and wrote the first draft of the paper. All authors contributed to the writing and interpretation. NSFC–NERC (Natural Environment Research Council of the United Kingdom) joint research program [nos. 41661134049 (to T.S.) and NE/P013805/1 (to P.J.V.).

Appendix A. Supplementary material

Supplementary material related to this article can be found online at https://doi.org/10.1016/j.epsl.2021.116903.

References

Acosta, R.P., Huber, M., 2020. Competing topographic mechanisms for the summer Indo-Asian Monsoon. Geophys. Res. Lett. 47.
Axelrod, D.I., 1965. A method for determining the altitudes of Tertiary floras. Paleobotanist 14, 144–171.
Axelrod, D.I., 1997. Paleoelevation estimates from Tertiary floras. Int. Geol. Rev. 39, 1124–1133.
Axelrod, D.I., Bailey, H.P., 1976. Tertiary vegetation, climate, and altitude of the Rio Grande depression, New Mexico–Colorado. Paleobiology 2, 235–254.
Bai, Y., Chen, C.H., Xu, Q., Fang, X.M., 2018. Paleoaltimetry potentiality of branched GDGTs from southern Tibet. Geochem. Geophys. Geosyst. 19, 551–564.
Barry, R.G., Chorley, R.J., 1987. Atmosphere, Weather, and Climate, 8th ed. Routledge, New York, p. 421.
Bolton, D., 1980. The computation of equivalent potential temperature. Mon. Weather Rev. 108, 1046–1053.
Boos, W.R., Kuang, Z., 2010. Dominant control of the South Asian monsoon by orographic insulation versus plateau heating. Nature 463, 218–222.
Botsyun, S., Sepulchre, P., Donnadieu, Y., Risi, C., Licht, A., Rugenstein, J.K.C., 2019. Revised paleoaltimetry data show low Tibetan Plateau elevation during the Eocene. Science 363, 946.
Coffinet, S., Huguet, A., Pedentchouk, N., Bergonzini, L., Omuombo, C., Williamson, D., Anquetil, C., Jones, M., Majule, A., Wagner, T., Derenne, S., 2017. Evaluation of branched GDGTs and leaf wax n-alkane delta H-2 as (paleo) environmental proxies in East Africa. Geochim. Cosmochim. Acta 198, 182–193.
Davies-Jones, R., 2008. An efficient and accurate method for computing the wet-bulb temperature along pseudoadiabats. Mon. Weather Rev. 136, 2764–2785.
DeCelles, P.G., Kapp, P., Quade, J., Gehrels, G.E., 2011. Oligocene-Miocene Kailas basin, southwestern Tibet: record of postcollisional upper-plate extension in the Indus-Yarlung suture zone. Geol. Soc. Am. Bull. 123, 1337–1362.
DeCelles, P.G., Quade, J., Kapp, P., Fan, M.J., Dettman, D.L., Ding, L., 2007. High and dry in central Tibet during the Late Oligocene. Earth Planet. Sci. Lett. 253, 389–401.
Deng, T., Wang, X.M., Wu, F.X., Wang, Y., Li, Q., Wang, S.Q., Hou, S.K., 2019. Review: implications of vertebrate fossils for paleo-elevations of the Tibetan Plateau. Glob. Planet. Change 174, 58–69.
Ding, L., Xu, Q., Yue, Y.H., Wang, H.Q., Cai, F.L., Li, S., 2014. The Andean-type Gangdese Mountains: paleoelevation record from the Paleocene-Eocene Linzhou Basin. Earth Planet. Sci. Lett. 392, 250–264.
Ehlers, T.A., Poulsen, C.J., 2009. Influence of Andean uplift on climate and paleoaltimetry estimates. Earth Planet. Sci. Lett. 281, 238–248.
Eiler, J.M., 2007. "Clumped-isotope" geochemistry - the study of naturally-occurring, multiply-substituted isotopologues. Earth Planet. Sci. Lett. 262, 309–327.
Eiler, J.M., 2011. Paleoclimate reconstruction using carbonate clumped isotope thermometry. Quat. Sci. Rev. 30, 3575–3588.
Farnsworth, A., Lunt, D.J., Robinson, S.A., Valdes, P.J., Roberts, W.H.G., Clift, P.D., Markwick, P., Su, T., Wrobel, N., Bragg, F., Kelland, S.J., Pancost, R.D., 2019. Past East Asian monsoon evolution controlled by paleogeography, not CO2. Sci. Adv. 5.
Feng, R., Poulsen, C.J., 2016. Refinement of Eocene lapse rates, fossil-leaf altimetry, and North American Cordilleran surface elevation estimates. Earth Planet. Sci. Lett. 436, 130–141.
Fluteau, F., 2003. Earth dynamics and climate changes. C. R. Geosci. 335, 157–174.
Foster, G.L., Royer, D.L., Lunt, D.J., 2017. Future climate forcing potentially without precedent in the last 420 million years. Nat. Commun. 8.
Gasson, E., Lunt, D.J., DeConto, R., Goldner, A., Heinemann, M., Huber, M., LeGrande, A.N., Pollard, D., Sagoo, N., Siddall, M., Winguth, A., Valdes, P.J., 2014. Uncertainties in the modelled CO2 threshold for Antarctic glaciation. Clim. Past 10, 451–466.
Ghosh, P., Garzione, C.N., Eiler, J.M., 2006. Rapid uplift of the Altiplano revealed through C-13-O-18 bonds in paleosol carbonates. Science 311, 511–515.
Gough, D.O., 1981. Solar interior structure and luminosity variations. Sol. Phys. 74, 21–34.
Held, I.M., Soden, B.J., 2006. Robust responses of the hydrological cycle to global warming. J. Climate 19, 5686–5699.
Huntington, K.W., Saylor, J., Quade, J., Hudson, A.M., 2015. High late Miocene-Pliocene elevation of the Zhada Basin, southwestern Tibetan Plateau, from carbonate clumped isotope thermometry. Geol. Soc. Am. Bull. 127, 181–199.
Jin, H.J., Chang, X.L., Wang, S.L., 2007. Evolution of permafrost on the Qinghai-Xizang (Tibet) Plateau since the end of the late Pleistocene. J. Geophys. Res., Earth Surf. 112.
Kattel, D.B., Yao, T.D., Yang, W., Gao, Y., Tian, L.D., 2015. Comparison of temperature lapse rates from the northern to the southern slopes of the Himalayas. Int. J. Climatol. 35, 4431–4443.
Liu, X.H., Xu, Q., Ding, L., 2016. Differential surface uplift: Cenozoic paleoelevation history of the Tibetan Plateau. Sci. China Earth Sci. 59, 2105–2120.
Lorenz, D.J., DeWeaver, E.T., 2007. Tropopause height and zonal wind response to global warming in the IPCC scenario integrations. J. Geophys. Res., Atmos. 112.
Lunt, D.J., Farnsworth, A., Loptson, C., Foster, G.L., Markwick, P., O'Brien, C.L., Pancost, R.D., Robinson, S.A., Wrobel, N., 2016. Palaeogeographic controls on climate and proxy interpretation. Clim. Past 12, 1181–1198.
Meyer, H.W., 1992. Lapse rates and other variables applied to estimating paleoaltitudes from fossil floras. Palaeogeogr. Palaeoclimatol. Palaeoecol. 99, 71–99.
Meyer, H.W., 2007. A review of paleotemperature - Lapse rate methods for estimating paleoelevation from fossil floras. Rev. Mineral. Geochem. 66, 155–171.
Minder, J.R., Mote, P.W., Lundquist, J.D., 2010. Surface temperature lapse rates over complex terrain: lessons from the Cascade Mountains. J. Geophys. Res., Atmos. 115.
Molnar, P., 2005. Mio-Pliocene growth of the Tibetan Plateau and evolution of East Asian climate. Palaeontol. Electronica 8.

Quade, J., Garzione, C., Eiler, J., 2007. Paleoelevation reconstruction using pedogenic carbonates. Rev. Mineral. Geochem. 66, 53–87.
Rolland, C., 2003. Spatial and seasonal variations of air temperature lapse rates in Alpine regions. J. Climate 16, 1032–1046.
Rowley, D.B., 2007. Stable isotope-based paleoaltimetry: theory and validation. Rev. Mineral. Geochem. 66, 23–52.
Rowley, D.B., Currie, B.S., 2006. Palaeo-altimetry of the late Eocene to Miocene Lunpola basin, central Tibet. Nature 439, 677–681.
Schildgen, T.F., Ehlers, T.A., Whipp, D.M., van Soest, M.C., Whipple, K.X., Hodges, K.V., 2009. Quantifying canyon incision and Andean Plateau surface uplift, southwest Peru: a thermochronometer and numerical modeling approach. J. Geophys. Res., Earth Surf. 114.
Sewall, J.O., Sloan, L.C., Huber, M., Wing, S., 2000. Climate sensitivity to changes in land surface characteristics. Glob. Planet. Change 26, 445–465.
Sherwood, S.C., Huber, M., 2010. An adaptability limit to climate change due to heat stress. Proceedings of the National Academy of Sciences 107, 9552–9555. Available online at: www.pnas.org/cgi/doi/10.1073/pnas.0913352107.
Smith, A.K., Marsh, D.R., Russell, J.M., Mlynczak, M.G., Martin-Torres, F.J., Kyrola, E., 2008. Satellite observations of high nighttime ozone at the equatorial mesopause. J. Geophys. Res., Atmos. 113.
Spicer, R.A., Farnsworth, A., Su, T., 2020a. Cenozoic topography, monsoons and biodiversity conservation within the Tibetan Region: an evolving story. Plant Divers.
Spicer, R.A., Herman, A.B., Kennedy, E.M., 2004. Foliar physiognomic record of climatic conditions during dormancy: Climate Leaf Analysis Multivariate Program (CLAMP) and the cold month mean temperature. J. Geol. 112, 685–702.
Spicer, R.A., Su, T., Valdes, P.J., Farnsworth, A., Wu, F.-X., Shi, G., Spicer, T.E.V., Zhou, Z., 2020b. Why 'the uplift of the Tibetan Plateau' is a myth? Nat. Sci. Rev.
Spicer, R.A., Yang, J., Spicer, T.E.V., Farnsworth, A., 2020c. Woody dicot leaf traits as a palaeoclimate proxy: 100 years of development and application. Palaeogeogr. Palaeoclimatol. Palaeoecol. 110138.
Stull, R., 2011. Wet-bulb temperature from relative humidity and air temperature. J. Appl. Meteorol. Climatol. 50, 2267–2269.
Su, T., Farnsworth, A., Spicer, R.A., Huang, J., Wus, F.X., Liu, J., Li, S.F., Xing, Y.W., Huang, Y.J., Deng, W.Y.D., Tang, H., Xu, C.L., Zhao, F., Srivastava, G., Valdes, P.J., Deng, T., Zhou, Z.K., 2019. No high Tibetan Plateau until the Neogene. Sci. Adv. 5.
Thayyen, R.J., Dimri, A.P., 2018. Slope Environmental Lapse Rate (SELR) of temperature in the monsoon regime of the Western Himalaya. Front. Environ. Sci.
Valdes, P.J., Armstrong, E., Badger, M.P.S., Bradshaw, C.D., Bragg, F., Crucifix, M., Davies-Barnard, T., Day, J.J., Farnsworth, A., Gordon, C., Hopcroft, P.O., Kennedy, A.T., Lord, N.S., Lunt, D.J., Marzocchi, A., Parry, L.M., Pope, V., Roberts, W.H.G., Stone, E.J., Tourte, G.J.L., Williams, J.H.T., 2017. The BRIDGE HadCM3 family of climate models: HadCM3@Bristol v1.0. Geosci. Model Dev. 10, 3715–3743.
Valdes, P.J., Lin, D., Farnsworth, A., Spicer, R.A., Li, S.H., Tao, S., 2019. Comment on "Revised paleoaltimetry data show low Tibetan Plateau elevation during the Eocene". Science 365.
Wang, Y., Deng, T., Biasatti, D., 2006. Ancient diets indicate significant uplift of southern Tibet after ca. 7 Ma. Geology 34, 309–312.
Wolfe, J.A., 1992. An analysis of Present-day terrestrial lapse rates in western conterminous United States and their significance to paleoaltitudinal estimates. USGS report 1964.
Wu, C., Yu, J.Z., 2018. Evaluation of linear regression techniques for atmospheric applications: the importance of appropriate weighting. Atmos. Meas. Tech. 11, 1233–1250.
Xiong, Z.Y., Ding, L., Spicer, R.A., Farnsworth, A., Wang, X., Valdes, P.J., Su, T., Zhang, Q.H., Zhang, L.Y., Cai, F.L., Wang, H.Q., Li, Z.Y., Song, P.P., Guo, X.D., Yue, Y.H., 2020. The early Eocene rise of the Gonjo Basin, SE Tibet: from low desert to high forest. Earth Planet. Sci. Lett. 543.
Zamora, R.A., Korty, R.L., Huber, M., 2016. Thermal stratification in simulations of warm climates: a climatology using saturation potential vorticity. J. Climate 29, 5083–5102.
Zhu, J., Poulsen, C.J., Tierney, J.E., 2019. Simulation of Eocene extreme warmth and high climate sensitivity through cloud feedbacks. Sci. Adv. 5.